IR Polarimetric Signatures

J. Larry Pezzaniti, David Chenault, Justin Vaden
Polaris Sensor Technologies

Kris Gurton, Melvin Felton
US Army Research Labs, Adelphi MD

Abstract

Infrared polarization relies on surface temperature, roughness, material properties, aspect angle to the sensor, sky down-welling and background radiance reflecting from the target. Often times, the polarization signature of a manmade target is different than the surrounding background. Furthermore, that difference is often present even when the thermal signature of the same target blends into the background. This paper will present maritime, airborne and ground data sets of polarization signatures of several objects that allow detection when other methods fall short.

1. Introduction

Acquiring and tracking a target is often performed using a Long Wave Infrared (LWIR) thermal imaging camera. In recent years, the cost of thermal imagers has dramatically reduced with the advent of microbolometer cameras, and is a very effective technology that fills the needs for many applications. Still, thermal imaging often falls short in situations involving high clutter and low thermal contrast.[1-4]

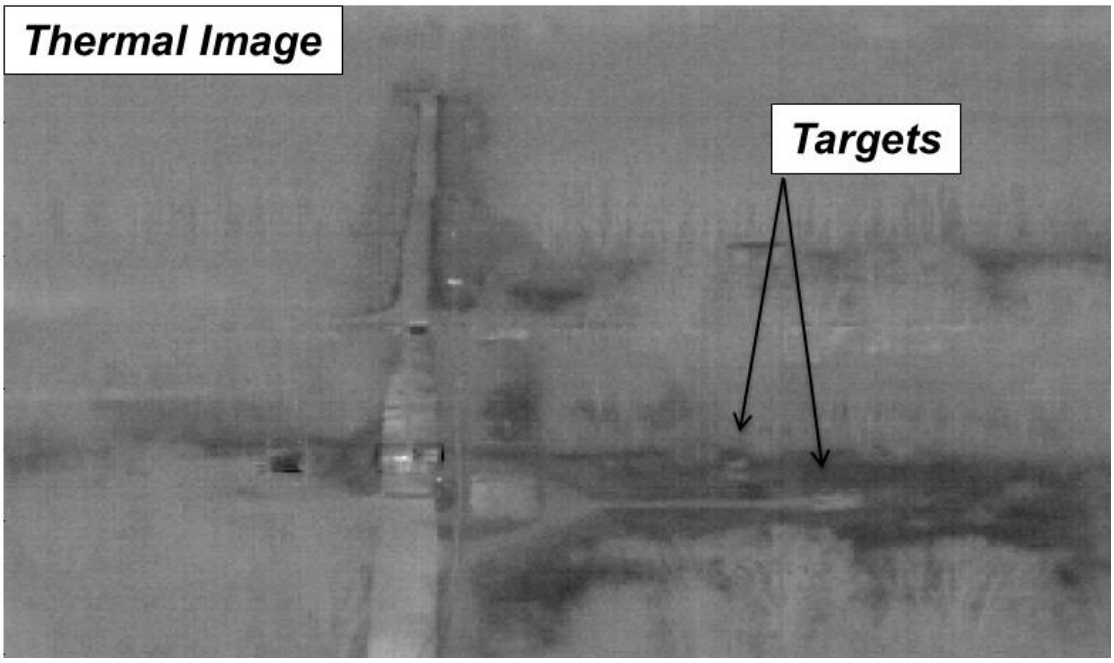

Figure 1 Standard LWIR thermal image of scene with two military targets. Image captured with a Corvus LWIR imaging polarimeter.

In this paper we present data from an LWIR imaging polarimeter that measures both the thermal and polarization content of an image. An imaging polarimeter is especially effective when thermal contrast is low or when the target becomes hidden in the background.

Figures 1 and 2 compare the thermal and polarization imagery taken from a Corvus LWIR imaging polarimeter offered by Polaris Sensor Technologies.[5] The image is taken from an altitude of 450 feet, approximately 1 km from the target. Both targets 1 and 2 are clearly visible in the IR polarized image. Target number 1 is also visible in the IR thermal image, but could easily be confused with several shrubs and other natural features surrounding Target 1. Target 2 completely blends into the roadway background and is not visible in the IR thermal image. Target 2 is only visible in the IR polarized image. Target 2 is invisible (zero contrast) in the IR thermal because it's apparent temperature equals the apparent temperature of the surrounding roadway. Zero contrast conditions often occur when the target has been at rest for several hours (no heat load from engine) or the target is camouflaged. Low contrast of 'at rest' or camouflaged targets is typically observed during two periods of the diurnal cycle. Those times depend primarily on the ambient temperature and solar loading profiles of a given day, along with parameters such as the thermal capacity and emissivity of the targets and backgrounds. Those times of day when the apparent temperatures of target and backgrounds are equal (zero contrast) are referred to as cross-over points. A significant advantage of polarimetry for target acquisition is that it still sees the target at those cross-over points.

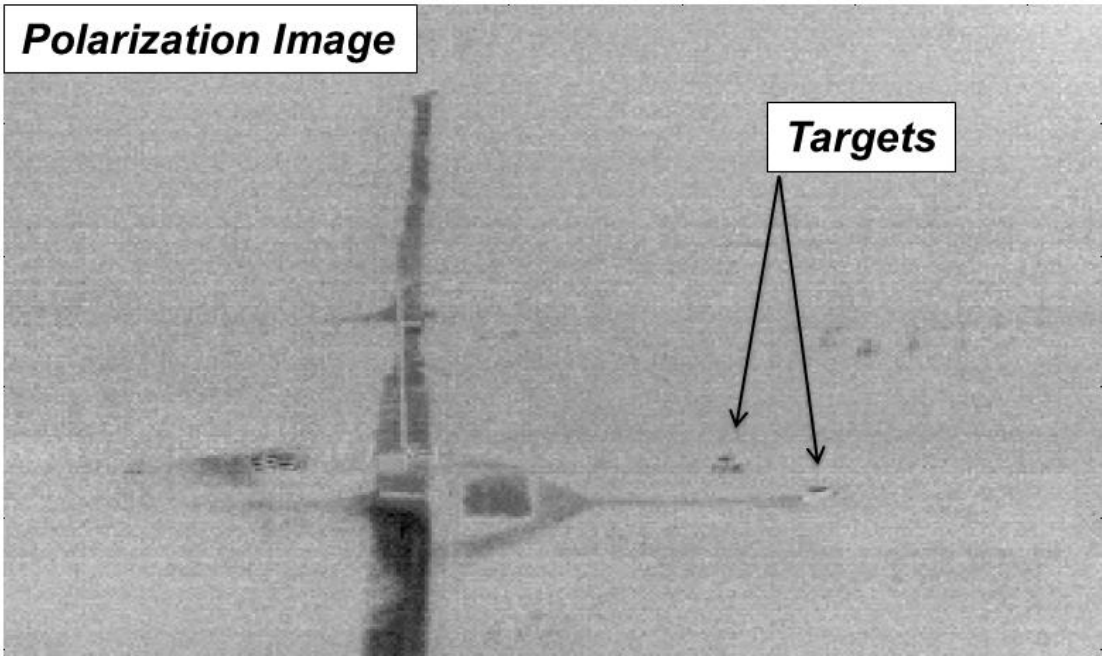

Figure 2 Polarimetric LWIR image of same scene as in **Figure 1**. Natural background of trees, shrubs, dirt, rocks is rejected in the polarized image because it is unpolarized. Military targets are partially polarized.

Another advantage of polarimetry is background clutter rejection. Note the complexity of the IR image compared to the Polarized image. Virtually all of the natural features such as trees, shrubs, large boulders, bald spots in the grass - all of which can take on the apparent size and temperature of a target of interest - are rejected in the polarized image. This level of discrimination from the sensor itself has the potential to greatly enhance the robustness of target acquisition, tracking and discrimination algorithms used in an air to ground seeker.

The physics that governs thermal and polarization signatures depends on the temperature, material and surface roughness of the target and background, the down-welling radiance, earth albedo, aspect angle, path radiance and several other parameters. Because these parameters change with waveband (either MWIR or LWIR), the thermal and polarization signatures also change with waveband. When polarization or thermal contrast is poor in the MWIR, it is often better in the LWIR and vice versa. Thus combining the MWIR and LWIR in one sensor can increase the robustness of detection tremendously.

2. Emission and Reflection Polarization

Thermal polarization is described in varying detail in the following references [6,7,8,9]. To understand the polarization signature of a surface it is instructive to develop the equations for polarized light emanating from a smooth surface. To understand thermal polarization, we must start with Kirkoff's law stating that spectral emissivity, ε of a surface equals spectral absorptivity, α of that surface and

$$\varepsilon(\lambda, T, \theta) = \alpha(\lambda, T, \theta) = 1 - r(\lambda, T, \theta), \quad (1)$$

where r is that surface's reflectance, λ is the wavelength of emission or reflected light, T is the temperature of that surface and θ is the angle of emission or reflection from the surface within the plane of incidence, see **Figure 3**. Two components of linear emissive or reflected polarization are defined to be parallel to the plane of incidence (defined by the reflected or emitted ray and the surface normal) and orthogonal to the plane of incidence. The corresponding Kirkoff's equations are

$$\varepsilon_{\parallel}(\lambda, T, \theta) = 1 - r_{\parallel}(\lambda, T, \theta) \quad (2)$$

$$\varepsilon_{\perp}(\lambda, T, \theta) = 1 - r_{\perp}(\lambda, T, \theta) \quad (3)$$

where $\parallel$ indicates emissivity or reflectivity of light linearly polarized in the plane of incidence and $\perp$ indicates emissivity or reflectivity of light linearly polarized perpendicular to the plane of incidence.

The polarization state of light emanating from a surface is composed of both emitted and reflected thermal radiation. The polarization state can be expressed as a Stokes vector in terms of the radiance values emerging from the surface.

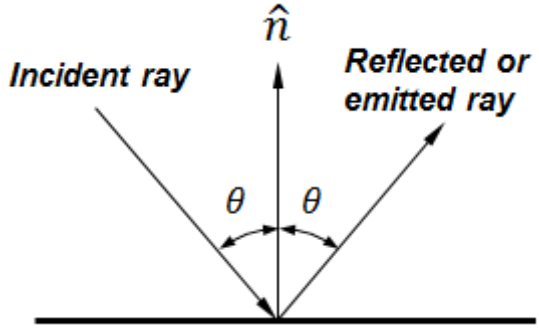

Figure 3 Angle of incidence

The Stokes vector is defined as,

$$\vec{S} = \begin{bmatrix} s_o \\ s_1 \\ s_2 \end{bmatrix} = \begin{bmatrix} L_\perp + L_\parallel \\ L_\perp - L_\parallel \\ L_{45} - L_{135} \end{bmatrix}. \quad (4)$$

$L_\parallel$ is the radiance of light polarized parallel to the plane of incidence given by

$$L_\parallel(\lambda, T, \theta) = \int_{\lambda_1}^{\lambda_2} \varepsilon_\parallel(\lambda, T, \theta) \cdot L_S(\lambda, T) \cdot d\lambda + \int_{\lambda_1}^{\lambda_2} r_\parallel(\lambda, T, \theta) \cdot L_B(\lambda, T) \cdot d\lambda \quad (5)$$

where λ_1 and λ_2 define the waveband of interest, $L_S(\lambda, T)$ is the blackbody radiation of the surface at temperature T, and $L_B(\lambda, T)$ is the background radiance reflected from the surface along the ray path within the plane of incidence defined by angle θ. Similarly,

$$L_\perp(\lambda, T, \theta) = \int_{\lambda_1}^{\lambda_2} \varepsilon_\perp(\lambda, T, \theta) \cdot L_S(\lambda, T) \cdot d\lambda + \int_{\lambda_1}^{\lambda_2} r_\perp(\lambda, T, \theta) \cdot L_B(\lambda, T) \cdot d\lambda \quad (6)$$

From equations (4), (5), and (6) we can write

$$s_1 = \int_{\lambda_1}^{\lambda_2} (r_\perp - r_\parallel) \cdot (L_B - L_S) \cdot d\lambda \quad (7)$$

where here we suppress the λ, T, θ dependencies to simplify the notation. Similarly we have

$$s_0 = \int_{\lambda_1}^{\lambda_2} (L_S + r \cdot (L_B - L_S)) \cdot d\lambda \quad (8)$$

The Stokes vector element s_2 appears when the plane of emission is rotated with respect to the detecting sensor.

To interpret these equations we can see that according to equation (7) for a smooth surface, a non-zero s_1 Stokes vector requires that the $L_B \neq L_s$ and $r_\perp \neq r_\parallel$. For many out-door situations, the condition $L_B \neq L_s$ is met, because surfaces tend to reflect sky background down-welling radiation that is significantly smaller than the emission of objects on the ground. For example, in the LWIR, if the sky apparent temperature is -20C, and the ground apparent temperature is 20C, then $L_B \sim \frac{1}{2} L_s$. On a cloudy summer day, the down-welling radiance can be closer to the emitted radiance of objects on the ground, but they will rarely be equal.

Secondly the parallel and perpendicular components of reflectance cannot be equal, $r_\perp \neq r_\parallel$. The difference $(r_\perp - r_\parallel)$ can be a strong function of surface roughness, the surface complex refractive index, angle of emissionθ, and wavelength λ. The difference $(r_\perp - r_\parallel)$ is a good source of contrast between an object of interest and its background. For example, for many man-made surfaces such as metal surfaces, glass, plastics, ceramics, this condition is met $r_\perp$ and $r_\parallel$ can differ by several percent. However, for many natural surfaces such as dirt, grass, trees, rocks, shrubs which are very rough, $r_\perp$ is nearly equal to or exactly equal to $r_\parallel$.

Thus the contrast in an image of s_1, which is based on the difference of $(r_\perp - r_\parallel)$ between the target of interest and the background, is often still significant even when the apparent temperature of the target equals the apparent temperature of the background.

Figure 4 compares a standard LWIR thermal image of a tank (s_o) to a LWIR polarized (s_1) of that same tank taken under exactly the same conditions. In the thermal image (s_o), the apparent temperature of the tank equals the apparent temperature of the background. However, in the s_1 polarization image still shows significant contrast.

It is important to note that an imaging polarimeter provides both thermal and polarization images and contrast is most often observed in at least one the two imaging modes.

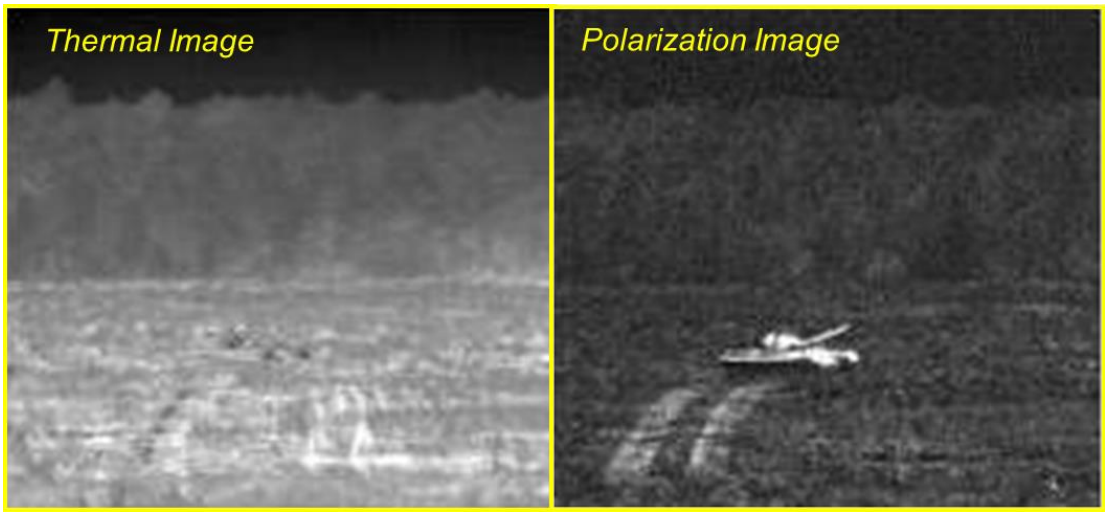

Figure 4 Comparison of thermal and polarization image.

3. Thermal Contrast vs Polarization Contrast

Figure 5 shows data from a LWIR imaging polarimeter. Two 18" x 18" Mylar panels are placed in an open field. The temperatures of the Mylar panels are controllable by passing current through resistive wire embedded in the Mylar. The Mylar panels are labeled 1 and 2 in the thermal images. The ambient temperature of the ground during this experiment was approximately 29C. The temperature of Mylar panel 1 was set to approximately 27C. The temperature of Mylar panel 2 was adjusted from just above 28C to approximately 29.5C. A movie of the panels was recorded over the course of about 1 minute as the temperature of Mylar panel 2 changed linearly from 28C to 29.5C. The imaging polarimeter recorded both thermal and polarization images at a rate of 30 fps from an altitude of 50ft at a standoff distance of approximately 300ft. Figure 5 is organized as follows. The top row is the three different thermal images corresponding to when Mylar panel 2 was at three different temperatures. The middle row shows the plots of the temperatures (sampled at 4 Hz) of the two panels and the ground over the 1 minute time frame. The bottom row is the thermal image with polarization overlaid in color. The left column shows the thermal and polarization images when Mylar panel 2 was cooler than the background, the middle column shows where the temperature of Mylar panel 2 equaled the background temperature, and the right shows Mylar panel 2 at a higher temperature than the background. Note that the polarization s_1 contrast remains high in spite of the thermal contrast passing through zero.

Figure 6 shows a plot of s_1 for Mylar panel 1 (held at 27C), Mylar panel 2 that changed temperature and the ground. Note that the polarization of the ground remained low <0.0025. The polarization of Mylar panel remained constant at approximately 0.035, and the polarization of Mylar panel 2 increased only slightly.

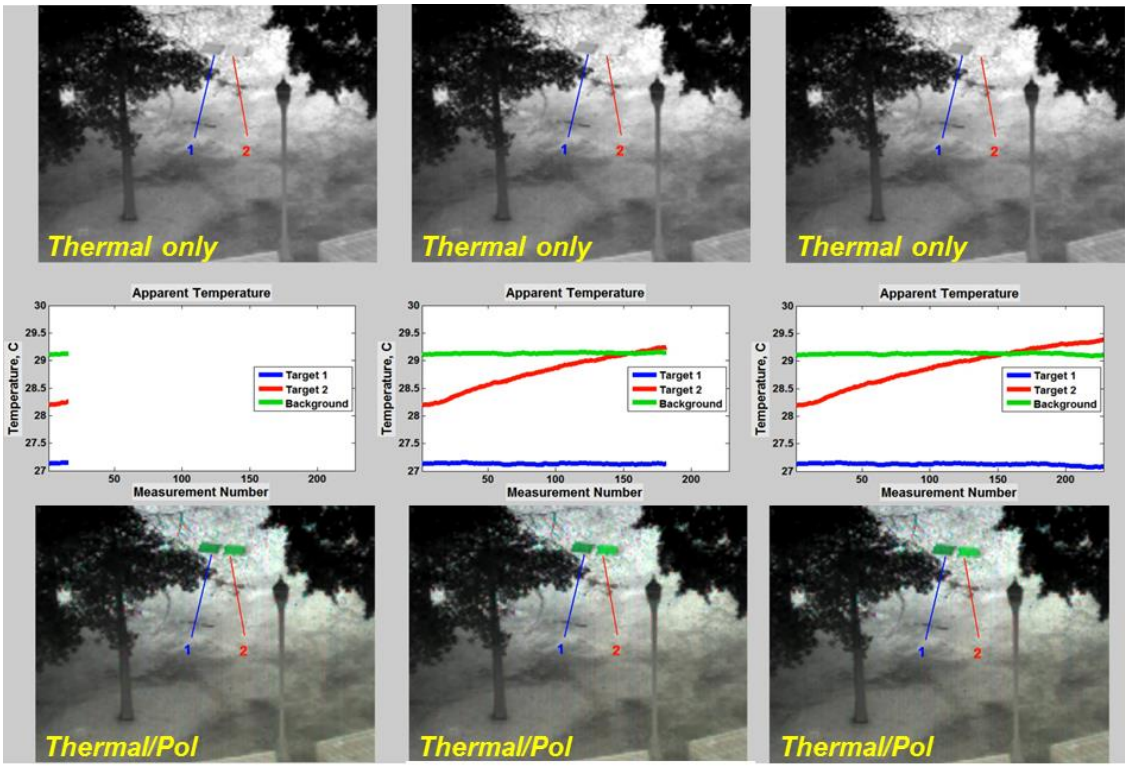

Figure 5 Polarization of targets during thermal cross-over point.

Figures 7 and **8** present another experiment where the LWIR imaging polarimeter was panned across an area of ground with several Mylar targets. The Mylar targets were adjusted to reach temperatures that matched the apparent temperature of the background.

In the thermal image, the five targets are very difficult to identify. Most of the observers that were showed the images could identify only two of the five targets.

Figure 8 shows the s_1 polarization image of the same targets take at the same instant. Of course all of the observers could identify all 5 targets. The polarization image is processed by painting pixels that show polarization above $s_1 > 0.02$ green. The unpolarized pixels remain grey level. The conditions for this test were clear sky with apparent sky temperature of approximately -30C. The ambient air temperature was approximately 25C. The sun azimuth with respect to the look angle was -90^o and elevation angle was 20^o.

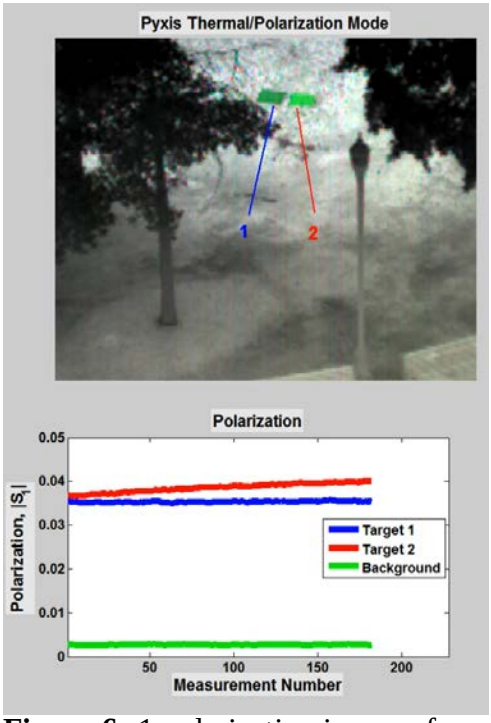

Figure 6 s1 polarization image of targets during thermal cross-over point.

Figure 7 Target set viewed in thermal mode

Figure 8 Target set viewed in thermal/polarization mode

4. Discussion and Conclusion

Thermal imagers fall short when the apparent temperature of an object of interest matches its surroundings or in situations involving significant background clutter. These conditions occur in many applications involving acquisition and tracking of ground vehicles in high clutter, UAV, UAS detection against sky and earth backgrounds, detection of swimmers and vessels on water backgrounds, and many other thermal applications.

An imaging polarimeter provides both polarization sensing *and* thermal sensing. When environmental conditions result in poor thermal contrast, the polarization mode often provides additional contrast even when thermal contrast is zero. In addition, since the detection physics of the polarization mode is different than the thermal mode, objects are often more easily visualized in the polarization mode or hybrid polarization/thermal mode. For example, when attempting to acquire a man-made object against an earth background, the natural earth background is largely rejected polarization allowing the man-made object to standout in the image.

With recent advances in polarimetry and the availability small SWAP imaging polarimeters, integration onto platforms such as UAS's, ground vehicles and un-mounted soldiers is now possible. The application space of LWIR imaging polarimetry is expected to grow significantly in the coming years.

References:

1. M. Felton, K. P. Gurton, J. L. Pezzaniti, D. B. Chenault, and L. E. Roth, "Measured comparison of the crossover periods for mid- and long-wave IR (MWIR and LWIR) polarimetric and conventional thermal imagery," Optics Express, Vol. 18, Issue 15, pp. 15704-15713 (2010).

2. C. An, J. Grantham, J. King, J. Robinson, L. Pezzaniti, K. Gurton, "Utility of Polarization Sensors for Clutter Rejection", 6th Annual US Missile Defense Conference, Washington DC, March 31-April 3, (2008).

3. K.P. Gurton, M. Felton, "Detection of buried Improvised Explosive Devices (IED) using passive long-wave infrared (LWIR) polarimetric imaging", ARL Technical Report, ARL-TR-4941 Sept. (2009).

4. J. S. Harchanko, D. B. Chenault, C. F. Farlow, and K. Spradley, "Detecting a surface swimmer using long wave infrared imaging polarimetry," in Photonics for Port and Harbor Security, M. J. DeWeert and T. T. Saito, eds., Proc. SPIE 5780 (2005).

5. www.polarissensor.com

6. S. Tyo, B.M. Ratliff, J. Boger, W. Black, D. Bowers, M. Fetrow, "The effects of thermal equilibrium and contrast in LWIR polarimetric images", Opt. Express, vol. 15, no. 23 Nov. (2007).

7. K.P. Gurton, M. Felton, "Detection of disturbed earth using passive LWIR polarimetric imaging" Proc SPIE Optics and Photonics Conference, San Diego, Ca. August 2-6, (2009).

8. O. Sandus, "A review of emission polarization," Appl. Opt. 4, 1634–1642 (1965).

9. K. P. Gurton, R. Dahmani, G. Videen, "Measured degree of infrared polarization for a variety of thermal emitting surfaces," Army Research Laboratory report , ARL-TR-3240, June 2004.